Spray-Coated Silver Nanowires as Top Electrode Layer in Semitransparent P3HT:PCBM-Based Organic Solar Cell Devices

Johannes Krantz, Tobias Stubhan, Moses Richter, Stefanie Spallek, Ivan Litzov, Gebhard J. Matt, Erdmann Spiecker, and Christoph J. Brabec*

Silver nanowire (Ag NW) thin films are investigated as top electrodes in semitransparent inverted organic solar cells. The performance of semitransparent poly(3-hexylthiophene-2,5-diyl):[6,6]-phenyl-C61-butyric acid methyl ester (P3HT:PCBM) organic solar cells with Ag NW top electrode layers is found to match very closely the performance of reference devices based on thermally evaporated, highly reflective metal silver top electrodes. The optical losses of the semitransparent electrodes are investigated in detail and analyzed in terms of transmission, scattering, and reflection losses. The impact on an external back reflector is shown to increase the light harvesting efficiency of optically thin devices. Further analysis of transparent devices under illumination from the indium tin oxide (ITO) backside and through the Ag NW front electrode open the possibility to gain deep insight into the vertical microstructure related devices performance. Overall, Ag NW top electrodes are established as a serious alternative to TCO based electrodes. Semitransparent devices with efficiencies of over $\eta = 2.0\%$ are realized.

1. Introduction

Transparent and conductive thin film electrodes are one of the most crucial components for thin film optoelectronic devices such as thin film solar cells, touch screens, or thin-film light-emitting diodes (organic light-emitting diodes (OLEDs) and others) for display and lighting applications. Today's state of the art electrodes for these applications are transparent doped metal oxides (TCOs). Indium doped tin oxide (ITO) is most frequently used for applications requiring high color neutrality (display, touch screen, lighting) whereas aluminium doped zinc oxide (AZO) is the standard electrode for thin film solar applications such as a-Si:H and CIGS. However and despite the outstanding performance of TCO electrodes, there are also some drawbacks of this material class. Some of them are fairly expensive (such as ITO electrodes), require elevated temperatures during the fabrication process (sputtering at >200 °C) and suffer from high brittleness in web-based applications. This web-based device design alleviates the need for intensive patterning of individual layers, like interfaces and photoactive layer. These drawbacks are less relevant for inorganic, glass based devices, but become more and more crucial for flexible substrate based devices like organic solar cells (OPV) or OLEDs.

Therefore the current generation of web-based optoelectronic devices has an urgent need for transparent electrodes that can be produced in large-scale, roll-to-roll and at low cost on flexible substrates, requiring low curing temperatures. Various material systems are currently in the focus of this research. Carbon allotrope based materials, like carbon nanotubes and graphene thin films are highly attractive with respect to costs, but currently still lack the required sheet resistance and transparency when compared to ITO.[1–5] Solution processed conducting oxides, processed from nanoparticles of sol-gel precursors either require high sintering temperatures (above 400 °C) or lack conductivity.[6] Highly doped organic solution processed polymers such as poly(3,4-ethylenedioxythiophene):poly(styrenesulfonate) (PEDOT:PSS) were demonstrated with conductivities above 1000 S/cm, resulting in conductivities of 40–80 Ohm/sq at transparencies of 85%. These polymer electrodes, in combination with metallic grid structures, were shown to come fairly close to the performance of ITO, even though they still did not meet the required 10 Ohm/sq at 85% transmission.[7–12]

Consequently conductive metal nanostructures have advanced in the focus of interest as replacements for doped metallic oxides in optoelectronic devices. Among these materials silver nanomaterials are the most promising candidates due to their outstanding electrical, thermal and optical properties.[13] As low

J. Krantz, T. Stubhan, M. Richter, I. Litzov, G. J. Matt, Prof. C. J. Brabec
Departement of Materials Science, I-MEET (WW6)
Friedrich-Alexander-University of Erlangen-Nuremberg
Martensstraße 7, 91058 Erlangen, Germany
E-mail: Johannes.Krantz@ww.uni-erlangen.de
S. Spallek, Prof. E. Spiecker
Center of Nanoanalysis and Electron Microscopy (CENEM)
Cauerstraße 6, 91058 Erlangen, Germany
Prof. C. J. Brabec
Bavarian Center for Applied Energy Research (ZAE Bayern)
Am Weichselgarten 7, 91058 Erlangen, Germany

DOI: 10.1002/adfm.201202523

temperature liquid processable materials, metallic nanostructures will be resource saving and, above all, energy conserving in compliance with the regulation of hazardous substances (RoHS). In consequence, metallic nanostructure electrodes are expected to advance TCO based electrodes in terms of manufacturing and material costs and, moreover, will be indium free. Besides the high attractivity from the processing point of view, metallic nanostructures further promise new opportunities in terms of light manipulation and light management. First investigations on metallic nanowire based layers indicate the possibility to in principle simultaneously satisfy the electrode requirements as well as enable controllable light management via plasmonic effects.[14,15] Plasmon effects can enhance the light output of OLEDs and, when ordered, the proposed silver nanowire electrodes can potentially polarize the emitted or transmitted light.[16,17] This degree of freedom might be provided by the design of silver nanomaterials in terms of being shaped into rods, wires, cubes and spheres.[18]

In recent years, among the various silver nanomaterials available, especially the silver nanowires have become a field with steadily increased research interest.[13,19–24] Numerous research reports on silver nanowires have been discussed their fascinating mechanical, optical and especially conductive properties.[14,25–27] As a percolation type electrode the conductivity follows a complex correlation between length and diameter (aspect ratio), as well as the area coverage by silver nanowires.[28–33] Furthermore silver nanowires exhibit many favourable properties as solution processable transparent electrodes for application in photovoltaics, LEDs and touch panels.[34,38]

Among the various applications envisaged for nanowire electrodes in organic electronics, organic photovoltaics is certainly the most mature one in terms of consumer products. Various exciting areas of application for light weight, low cost and highly flexible solar cell devices are currently emerging, which cannot be addressed by brittle TCO-based electrodes. However silver nanowires already appear in several consumer products, one of which is touch panels for mobile phone application. Building integrated applications (BIPV) fitting well to semitransparent solar cells, which require two transparent electrodes. These electrode structures are currently developed with various designs of screen or flexo printed metallic grids, but would certainly benefit from a highly conductive, highly transparent, thin and flat (as opposed to the issues with elevations that grid-based approaches have) one component electrode rather than a hybrid electrode.[39] Gaining access to such favorable electrode structures is expected to prime the path of OPV towards novel applications like aesthetic interior designed photovoltaics or to functionalized surfaces as envisaged in buildings and automotive applications.[40]

In this manuscript we analyze the optical properties of solution processed Ag NWs as top electrode layer in semitransparent solar cell devices and demonstrate the feasibility of such a percolation type of metallic nanostructures for top electrode applications. Recently Yang and co-workers demonstrated the fabrication of Ag NW as transparent electrodes for semitransparent organic photovoltaic devices.[41] The solution based deposition is a critical step in the OPV process, since diffusion of the metallic nanostructures into the bulk may shunt the whole device. Nanoparticular silver inks are typically low viscosity water or alcohol based dispersions and, as such, specifically susceptible to this defect. Girotto and co-workers found an elegant engineering solution around this general problem and suggested spray coating as a suitable process for the deposition of nanoparticular Ag inks.[42]

Here we present our findings on the incorporation of spray coated silver nanowire layers as transparent top electrodes into P3HT:PCBM based inverted solar cells. With the exception of the bottom electrode, these devices were fully solution processed with a combination of doctor blading and spray coating, both being methods compatible to roll-to-roll processing.

The overall performance of the top processed electrodes was of comparable quality to previously reported, solution processed Ag NW bottom electrodes. Overall this established solution processed Ag NW electrodes as a highly attractive ITO alternative.[19]

2. Experimental Section

The semitransparent solar cell devices presented in this work have been fabricated according to the architecture introduced in **Figure 1**.

On top of 1 mm thick glass substratesindium tin oxide (ITO) with 5 Ohm/square (Ω/sq) was sputtered by an external supplier and laser patterned in our labs. All layers except the top electrode were deposited by doctor blading in ambient atmosphere. Since the devices were realized in the inverted architecture, ITO was first functionalized by application of a metal oxide. In this case a thin (≈40 nm) electron injecting layer (EIL) composed of aluminum-doped zinc oxide (AZO) was chosen to enable electron selective charge carrier collection. The low temperature AZO route was prepared as reported previously.[43] On top of the AZO interface a 2 wt% P3HT:PCBM blend from chlorobenzene (CB) was deposited with a nominal thickness of around 100 nm. The semiconductor layer thickness was chosen to be fairly thin to realize transparent devices. A thin layer of PEDOT:PSS (HC Stark, PEDOT AL4083) was then coated on top of the active layer. PEDOT:PSS serves on one hand as hole collector with average electron blocking properties and further protects the semiconductor layer from shunting effects, both for thermally evaporated silver as well as spray coated Ag NWs. Typical thicknesses of the PEDOT:PSS interface layer are

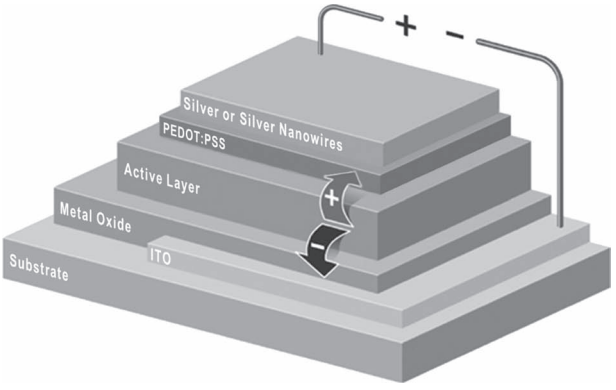

Figure 1. Device architecture for the inverted organic solar cell. The top electrode was either thermally evaporated silver or spray-coated silver nanowires. Due to the Ag NWs outstanding transmittance these devices are semitransparent.

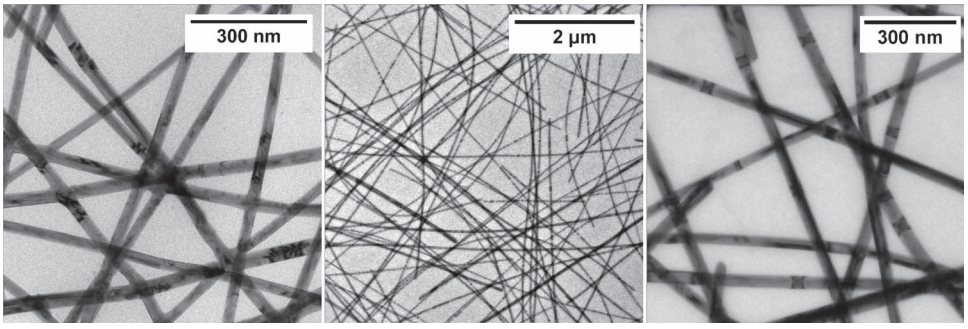

Figure 2. A typical layer of spray coating deposited silver nanowires is presented (left). For comparison a typical doctor bladed electrode layer is presented on an overview (middle) and a comparable zoom (right). The high similarity between spray coating and the doctor blading technique is confirmed for Ag NW layer quality and morphology. As observed in our previous report bend contours of the Ag NWs lead to variations for the Bragg-contrast.[19]

30–40 nm. Before application of the individual final electrode layers the devices were thermally treated in a nitrogen atmosphere at 140 °C for 5 min to remove remaining solvents.[44]

Reference devices were finished with a thermally evaporated silver top electrode layer of 100 nm thickness, which also performs as a back reflector due to the rather thin semiconductor layer. This device architecture regularly reaches power conversion efficiencies (PCE) of up to $\eta \approx 3\%$. Higher efficiencies require larger semiconductor thickness.

Ag NW electrode layers have been spray deposited by a custom-built spray coating setup. Spray coating was chosen for Ag NW deposition to minimize drying effects at the Ag NW–PEDOT:PSS interface and to reduce the overall drying times. Earlier attempts of device fabrication via doctor blading showed poor layer compatibility between the PEDOT:PSS and the AG NW ink due to the aqueous nature of both materials. In addition, doctor blading requires post structuring of the top electrode. Alternatively spray coating allowed us to spray through a shadow mask, directly yielding devices with the required active device area of 10.4 mm^2. However commercial production spray-coating systems are available that do the spray-coating itself in a patterned manner, making electrode patterning by shadow masks unnecessary. The typical optoelectronic properties of these Ag NW layers exhibit a sheet resistance of approx. 7 Ω/sq and an average transmission of over 85% between 400–800 nm in the visible light spectrum. Transmission electron microscopy (TEM) investigations (**Figure 2**) further proved that doctor bladed and spray coated nanowire electrodes are essentially identical, not only from their optoelectronic properties but also from their microstructure and morphology as well as percolation.

Spectroscopic data on the total, direct and diffuse transmission as well as reflection and absorption were obtained with a Perkin Elmer Lambda 950 high performance double beam spectrometer including an integrating sphere.

All solar cell devices were encapsulated to avoid degradation in air and evaluated at 100 mW cm^{-2} illumination with an AM1.5 solar spectrum from a Newport Sol1A 94061 solar simulator. The solar simulator was calibrated by a cristalline Si-cell before measurement. In addition, a shadow mask was used to confine illumination to the active area only.

3. Results

We have recently introduced optical modeling to better understand the color appearance of transparent solar cells.[45] Following this model, transmission spectroscopy on transparent solar cells from either electrode side as well as the overall transparency of the solar cell can be analyzed as a mix of various effects. By optimizing the interference effects being induced from the bottom metal oxide the optical losses at the various electrodes can be further reduced. Previous experiments for a PEDOT:PSS/Ag grid electrode showed that this electrode can be optimized to having only 5–10% more absorption than a corresponding ITO-based one.[12]

To learn about the optical properties of the spray coated Ag NW electrode layers, the transmission of fully processed devices was taken from both sides, one time via the ITO/ZnO electrode, the other via the Ag NW/PEDOT:PSS electrode. If not stated otherwise, the solar cells have been illuminated through the bottom ITO electrode layer.

Figure 3 presents a comparison of absorption (optical density, OD) for a solar cell device with Ag NW top electrode.

The device in Figure 3a was illuminated from the top and the back of the substrate, either through the Ag NWs or ITO electrode. Most interestingly we found more or less identical transmission, or optical density (OD) respectively, from both sides. The OD reported in Figure 3b was derived from the total transmission, e.g. the sum from direct and diffuse transmission, as measured at the entrance of an integrating sphere. To verify this behavior, large area device structures with active areas of over 1 cm^2 were built and characterized. Again Figure 3b proves that the total transmission was identical from either electrode side. For illumination through Ag NWs we had expected a significant reflection contribution due to the silver plasmon resonance at a wavelength of 380 nm.[19] However we were not able to observe any significant differences in transmission for either direction of illumination. Obviously the reflection losses at both transparent electrodes as well as their interfaces are considerably small so that the optical properties of the devices are controlled by the absorption of the individual layers rather than interference effects.

Next the impact of diffuse scattering from the Ag NW layer was analyzed. The direct transmission of semitransparent

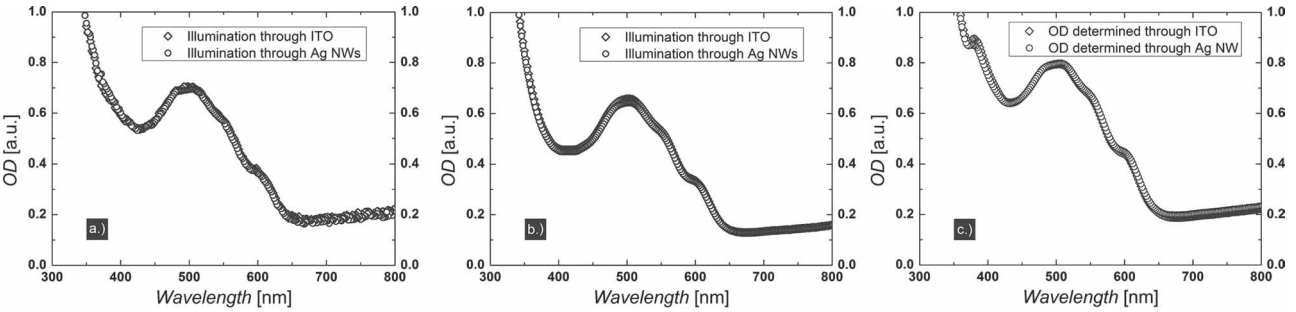

Figure 3. Optical properties of a semitransparent P3HT:PCBM solar cell device, OD from total transmission in front of the integrating sphere. a) A mask was employed on a 10 mm^2 active area device. b) Illumination of 1 cm^2 semitransparent device. c) OD from direct transmission only of 1 cm^2 device. Illumination was done through ITO or the Ag NW electrode respectively. The absorption of the Ag plasmon is clearly seen in Figure 4 at around 380 nm (silver plasmon resonance wavelength). However identical absorption spectra were observed under either illumination side, suggesting the plasmon absorption and not the plasmon reflection is decisive. Slight spectral variance around 500 nm is expected due to thickness variation in the active layer material and the investigated spot on the sample.

devices was measured with an optical path length between sample and the front entrance of the integrating sphere of approximately 65 cm, only collecting photons transmitted within an angle of 0.7°. Figure 3c shows that the OD determined from direct transmission was approximately 25% higher than from total transmission (OD of 0.8 rather than 0.6). From visual inspection the overall haze of the devices was fairly low. As soon as the Ag nanowires are cladded with a low index medium like PVP, reflection as well as scattering was suppressed.

To further investigate and better understand the optical properties of the nanowire electrodes, a full set of transmission and reflection spectra were taken for both illumination directions (Ag NW/glass vs. glass/Ag NW). The sample consisted of the Ag NW electrode layer on glass only to make sure no interference from the solar cell stack does obscure the results. Absorption (A) was measured with the sample aligned under a small angle (8°) inside the integrating sphere, reflection (R) was measured with the sample at the rear port of the sphere, total and diffuse transmission (T) were measured with the sample at the entrance port of the sphere. In case of diffuse transmission the back port white reflector was removed to let the direct transmission pass through the sphere, yielding only the diffuse part of the transmission. According to $A + T + R = 1$, the total sum of all individual spectra has to add up to 1 (100%). This was verified for all measurements and the spectral dependence of the deviations was found to be less than 1%, thus proving the high precision of these measurements.

Figure 4 summarizes the optical properties of the Ag NW electrode for both illumination directions. Only small differences are observed upon changing the illumination direction. The most prominent change was a small shift in the reflection/absorption contributions at the plasmon resonance frequency between 350–380 nm. Illumination through the glass results in a strong plasmon absorption, while illumination through the Ag NWs shows a stronger plasmon reflection. The difference in these contributions was approximately 7% for the respective illumination direction. As already mentioned above, diffuse transmission was comparable for both illumination directions and the spectrally resolved haze was in an acceptable regime for solar cell applications.

Having understood the optical properties of the Ag NW electrodes, we next analyzed the solar cell performance as a function of the illumination direction. A set of measurements

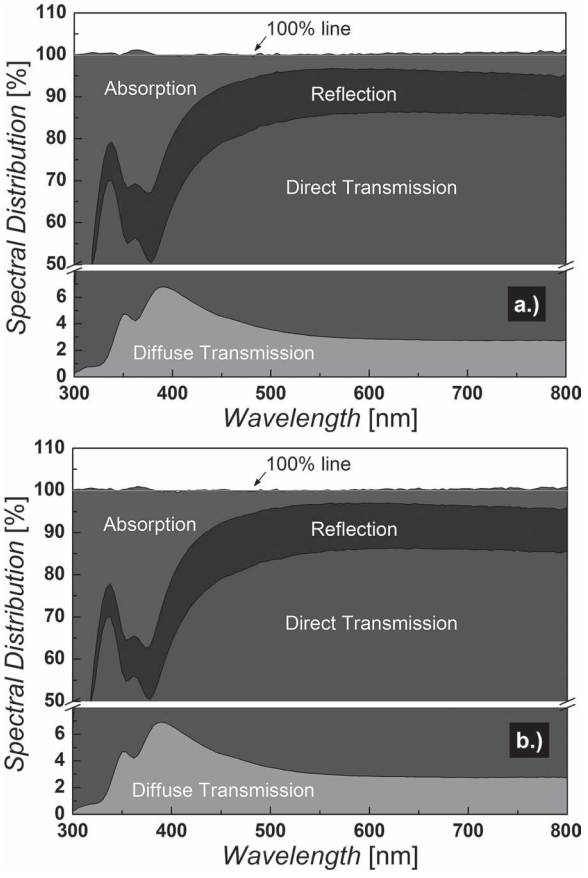

Figure 4. Optical properties of Ag NW electrodes on glass. a) Spectrally resolved absorption, reflection and transmission properties of a Ag NW layer when illuminated from the glass side. The diffuse transmission is magnified. b) Spectrally resolved optical properties of the same electrode when illuminated from the Ag NW side. As a control for the precision of the measurements, the sum of A, T and R is plotted in both figures proving that the deviation from the 100% is less than 1%.

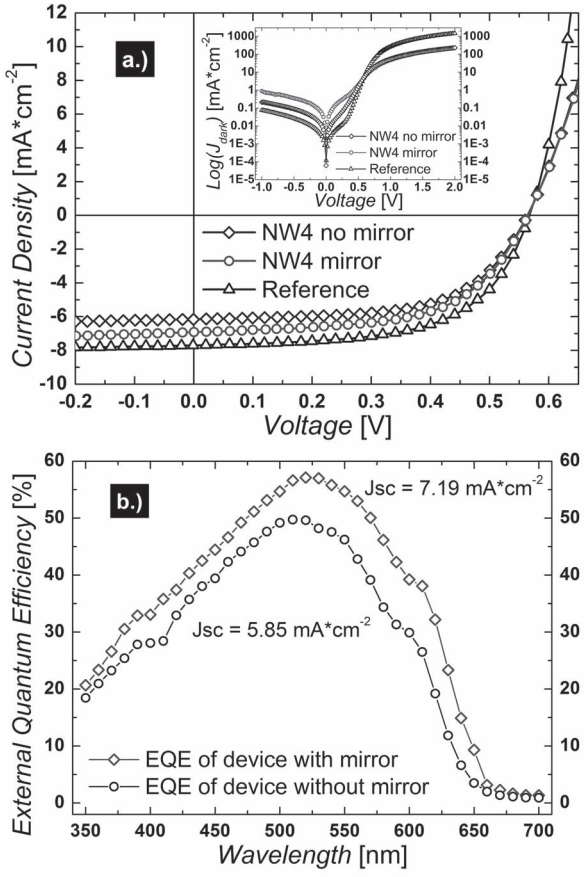

Figure 5. a) The semitransparent device performance with Ag NW electrode is compared to a reference device with thermally evaporated Ag top electrode layer. Performance of these devices: PCEs of $\eta_{Ag} = 2.6\%$, $\eta_{AgNW} = 2.1\%$ and $\eta_{AgNW,mirror} = 2.3\%$. $V_{oc} = 0.56$ V for both devices, $J_{sc,Ag} = 7.7$ mA cm^{-2}, $J_{sc,AgNW} = 6.1$ mA cm^{-2} and $J_{sc,AgNW,mirror} = 6.9$ mA cm^{-2}. FF of 60.6% for ITO device, 60.6% for Ag NW cell and 59% for Ag NW cell measured with mirror were observed, serial resistances (R_s) are $R_{s,Ag} = 0.7$ Ω cm^2 and $R_{s,AgNw} = R_{s,AgNW,mirror} = 5.3$ Ω cm^2, parallel resistances (R_p) of $R_{p,Ag} = 25$ kΩ cm^2, $R_{p,AgNW} = 1.2$ kΩ cm^2 and $R_{p,AgNW,mirror} = 6.5$ kΩ cm^2, the photoshunts of $R_{p,photo,Ag} = 1.2$ kΩ cm^2, $R_{p,photo,AgNW} = 1.4$ kΩ cm^2 and $R_{p,photo,AgNW,mirror} = 0.8$ kΩ cm^2. b) EQE spectra for the device presented in Figure 6. The achieved performances of semitransparent solar cell devices with Ag NW top electrode layer is confirmed and are in good agreement with AM 1.5 spectrum with and without mirror.

always contained the characterization of a transparent device from both illumination directions together with the characterization of a non-transparent, but otherwise identical device.

Figure 5a compares the current–voltage (*J-V*) characteristics of a semitransparent solar cell with one from a reference device. In general a semitransparent device is always expected to show a lower short circuit current (J_{sc}) density due to the missing reflection from the back electrode leading to reduced absorption for nearly all situations. The interplay of absorption, back reflection and thin film interference was analyzed in great detail by Ameri et al.[45] For most thin film devices the silver top electrode in regular solar cell devices acts as a fairly efficient back reflector. Depending on the refractive index and the thickness of the interface layer, reflected light can be focused into the semiconductor, leading to enhanced absorption. Semitransparent cells are missing this contribution. To demonstrate that this multi-absorption effect indeed was relevant in our solar cells, a planar mirror was placed behind the solar cells to reflect the otherwise transmitted and lost light. Although the reflection from such a mirror was expected to overall increase absorption in the solar cell, these effects not necessarily need to be comparable to reflection from the back electrode. The reason for that are the thin film interferences, which are absent for an external back reflector.[45] According to Figure 5 the short circuit current of a transparent device was almost 2 mA cm^{-2} less than for an opaque device with a reflecting Ag electrode. Placing a mirror at the backside of the cell brings back almost 1 mA cm^{-2}. A similar increase in J_{sc} has been confirmed by external quantum efficiency (EQE) evaluation (Figure 5b). The achieved device performances are in excellent agreement for EQE measurements and evaluation under AM 1.5 solar spectrum. The other performance parameters such as fill factor (FF) or open circuit voltage (V_{oc}) are almost identical for both devices. Noteworthy is the difference in serial resistance (R_s) and in parallel resistance (R_p) of the Ag NW electrode based devices.[44,45] Despite the high conductivity of the Ag NW electrode of 7 Ohm/sq, R_s was almost 5 times higher than for the opaque Ag electrode. This is visualized in Figure 5, where the Ag NW devices show significantly reduced current injection in the first quadrant.

Surprisingly the very high serial resistance for the semitransparent device does not seem to significantly impair the solar cells FF. In general a serial resistance of 1 Ohm cm^2 is assumed to be the critical value upon when Rs is starting to negatively impact the FF.[46,47] The discrepancy between the high series resistance despite a rather low "lateral" electrode resistance is typically explained by a high contact resistance limiting current injection.

In this context, it is interesting to further discuss potential Rs contributions in percolation type electrodes. Bulk electrode layers offer nearly identical sheet resistances across the whole

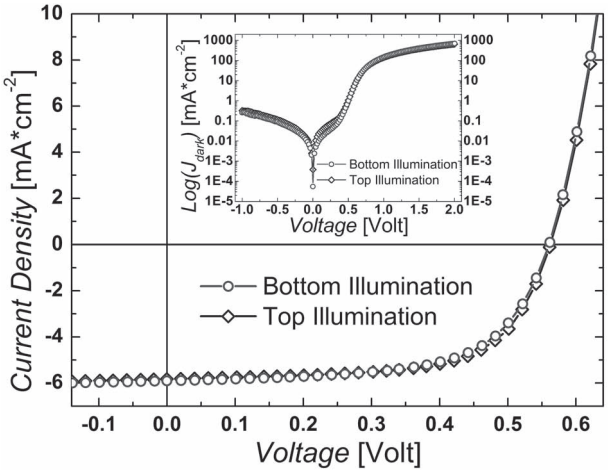

Figure 6. *J–V* characteristics of a device illuminated through the ITO and the Ag NW electrode. Identical J_{sc} was observed for both illumination directions. Performances: $\eta_{Top} = 2.13\%$, $\eta_{bottom} = 2.07\%$, $V_{oc} = 0.56$ V for both devices, $J_{sc,top} = 5.83$ mA cm^{-2} vs. $J_{sc,bottom} = 5.91$ mA cm^{-2}, $FF_{top} = 65.1\%$ vs. $FF_{bottom} = 62.6\%$, $R_{s,top} = 1.82$ Ω cm^2 vs. $R_{s,bottom} = 1.68$ Ω cm^2, $R_{p,top} = 4.7$ kΩ cm^2 vs. $R_{p,bottom} = 8.3$ kΩ cm, $R_{p,photo,top} = 1.40$ kΩ cm^2 vs. $R_{p,photo,bottom} = 1.36$ kΩ cm^2.

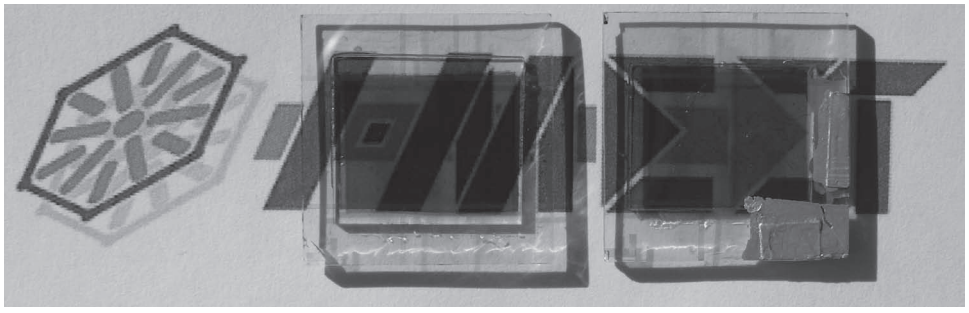

Figure 7. Photograph of the semitransparent devices discussed in this manuscript. The performance of the device on the left is presented in Figure 5a, the EQE for the device on the right in Figure 5b and its performance in Figure 6. The high transmittance of the electrode layer makes it difficult to identify them, but underlines the outstanding optical properties of the NW electrode. Each substrate contains six separate devices.

electrode layer. For percolation type electrodes this picture is different. Areas with a nearby nanowire offer good charge collection properties. For void areas in between the nanowires charge collection may be limited by the significantly poorer transport properties of the interface material. For both scenarios, the contact resistance between the interface layer and the nanowires does contribute to the total series resistance.

The slight reduction in fill factor of the device evaluated with a mirror is attributed to the reduced photoshunt, i.e., the reduced parallel resistance under illumination.[46] $R_{p,photo}$ was reduced from 1.4 kΩ cm^2 to 0.8 kΩ cm^2. This is likely to come from repeated *J–V* measurements under forward and reverse bias. Degradation due to oxygen or water ingress can be excluded as the origin for the FF variation. For unencapsulated devices with Ag NW top electrode we observed fast photocurrent degradation within a few minutes under 100 mW cm^{-2} illumination in air. This is in good agreement with the findings of investigations into water and oxygen leaking electrodes, which reported photo oxidation of the P3HT:PCBM blend as the dominant degradation process.[48,49]

Figure 6 compares the performance of a semitransparent device when illuminated through the top (Ag NW) or bottom (ITO) electrode. The *J–V*-curves presented here show no significant differences in terms of J_{sc} or V_{oc}. Although other studies on transparent solar cells reported different findings, this is actually in excellent agreement with our findings from the transmission measurements.[50] The only difference was a slight improvement in the FF under illumination through the Ag NW top electrode. These differences are certainly small, but could reflect an interesting specific property of organic solar cells, namely the significant differences in hole and electron mobilities of bulk heterojunction composites. Similar effects were analyzed for amorphous silicon.[51,52] Alternatively different surface recombination velocities at the two electrodes might also cause such small deviations in the FF. Further investigations are required to finally clarify these small FF variations upon illumination from the front vs. back side.

Finally **Figure 7** presents pictures of the semitransparent devices which have been discussed in this manuscript. No or only little haze was observed, in good agreement with the low scattering caused by the presented Ag NW electrode layers. The devices presented in Figure 7 highlight the outstanding transparency of the semitransparent solar cells. Together with the good electrical properties, the high FF and high current collection properties, this again proves the high potential of Ag NW electrodes to replace ITO.

4. Summary

In this report we present semitransparent P3HT:PCBM based solar cells. A silver nanowire percolation type electrode provides the highly conductive and transparent top contact in an inverted device architecture. The performance of these semitransparent devices was found to closely match the reference solar cell device with thermally evaporated silver top electrode. Remaining slight performance differences can be attributed to the reduced absorption in the semitransparent device configuration and the therefore lowered J_{sc}. This has further been confirmed by EQE investigations. Most interestingly these devices exhibit nearly identical optical as well as device performance properties upon illumination from either side.

Acknowledgements

The authors gratefully acknowledge the financial support from AiF Projekt GmbH. T.S. was funded by a German Research Foundation project grant (DFG; BR 4031/1-1). This work has further been financially supported by the Engineering of Advanced Materials excellence cluster (EAM), University of Erlangen-Nuremberg. The authors are very grateful to Cambrios Technology Corporation for their supply of specially made ClearOhm Ink for this study.

Received: September 3, 2012
Published online: October 26, 2012

[1] Y. Wang, S. W. Tong, X. F. Xu, B. Özyilmaz, K. P. Loh, *Adv. Mater.* **2011**, *23*, 1514.
[2] J. L. Blackburn, T. M. Barnes, M. C. Beard, Y. Kim, R. C. Tenent, T. J. McDonald, B. To, T. J. Coutts, M. J. Heben, *ACS Nano* **2008**, *2*, 1266.
[3] A. A. Green, M. C. Hersam, *Nano Lett.* **2008**, *8*, 1417.
[4] M. W. Rowell, M. A. Topinka, M. D. McGehee, H. J. Prall, G. Dennler, N. S. Sariciftci, L. Hu, G. Gruner, *Appl. Phys. Lett.* **2006**, *88*, 233506.
[5] J. Wu, H. A. Beverril, Z. Bao, Z. Liu, Y. Chen, P. Peumans, *Appl. Phys. Lett.* **2008**, *92*, 263302.

[6] S. Schoemaker, A. Rosin, T. Gerdes, M Willert-Porada, T. Lüthge, *Eur. J. Glass Sci. Technol. Part A* **2009**, *50*, 82.
[7] A. Colsmann, M. Reinhard, T. H. Kwon, C. Kayser, F. Nickel, J. Czolk, U. Lemmer, N. Clark, J. Jasieniak, A. B. Holmes, D. Jones, *SOLMAT* **2011**, *98*, 118.
[8] C. N. Hoth, R. Steim, P. Schilinsky, S. A. Choulis, S. F. Tedde, O. Hayden, C. J. Brabec, *Org. Electron.* **2009**, *10*, 587.
[9] F. C. Krebs, *SOLMAT* **2009**, *93*, 1636.
[10] Y. Zhou, F. Li, S. Barrau, W. Tian, O. Inganäs, F. Zhang, *SOLMAT* **2009**, *93*, 497.
[11] Y. Zhou, F. Zhang, K. Tvingstedt, S. Barrau, F. Li, W. Tian, O. Inganäs, *Appl. Phys. Lett.* **2008**, *92*, 233308.
[12] J. Zou, H.-L. Yip, S. K. Hau, A. K.-Y. Jen, *Appl. Phys. Lett.* **2010**, *96*, 203301.
[13] J. Lee, S. T. Connor, Y. Cui, P. Peumans, *Nano Lett.* **2008**, *8*, 689.
[14] H. Ditlbacher, A. Hohenau, D. Wagner, U. Kreiwig, M. Rogers, F. Hofer, F. R. Aussenegg, J. R. Krenn, *Phys. Rev. Lett.* **2005**, *95*, 257403.
[15] X. Li, W. C. H. Choy, L. Huo, F. Xie, W. E. I. Sha, B. Ding, X. Guo, Y. Li, J. Hou, J. You, Y. Yang, *Adv. Mater.* **2012**, *24*, 3046.
[16] Z. Li, K. Bao, Y. Fang, Y. Huang, P. Nordlander, H. Xu, *Nano Lett.* **2010**, *10*, 1831.
[17] L. L. Wang, Chang-Ling Zou, X. F. Ren, A. P. Lui, L. Lv, Y. J. Cai, F. W. Sun, G. C. Guo, G. P. Guo, *Appl. Phys. Lett.* **2011**, *99*, 061103.
[18] A. Graff, D. Wagner, H. Ditlbacher, U. Kreibig, *Eur. Phys. J. D* **2005**, *34*, 263.
[19] J. Krantz, M. Richter, S. Spallek, E. Spiecker, C. J. Brabec, *Adv. Funct. Mater.* **2011**, *21*, 4784.
[20] W. Gaynor, J. Y. Lee, P. Peumans, *ACS Nano* **2009**, *4*, 30.
[21] W. Gaynor, G. F. Burkhard, M. D. McGehee, P. Peumans, *Adv. Mater.* **2011**, *23*, 2905.
[22] S. E. Shaheen, M. S. White, D. C. Olsen, N. Kopidakis, D. S. Ginley, *SPIE Newsroom* **2007**.
[23] J. Y. Lee, S. T. Connor, Y. Cui, P. Peumans, *Nano Lett.* **2010**, *10*, 1276.
[24] L. Hu, H. S. Kim, J. Y. Lee, P. Peumans, Y. Cui, *ACS Nano* **2010**, *4*, 2955.
[25] V. Rodrigues, D. Ugarte, *Phys. Status Solidi B* **2001**, *230*, 475.
[26] C. A. Stafford, *Phys. Status Solidi B* **2001**, *230*, 481.
[27] G. Baffou, R. Quidant, C. Girard, *Appl. Phys. Lett.* **2009**, *94*, 153109.
[28] D. Simien, J. A. Fagan, W. Luo, J. F. Douglas, K. Migler, J. Obrzut, *ACS Nano* **2008**, *2*, 1879.
[29] C. Hong, X. Yu, *Nanoscale Res. Lett.* **2011**, *6*, 1.
[30] A. Benahm, A. Ural, *Phys. Rev. B* **2007**, *75*, 125432.
[31] A. R. Madaria, A. Kumar, F. N. Ishikawa, C. Zhou, *Nano Res.* **2010**, *3*, 564.
[32] S. Kumar, J. Y. Murthy, M. A. Alam, *Phys. Rev. Lett.* **2005**, *95*, 066802.
[33] J. Hicks, A. Benham, A. Ural, *Phys. Rev. E* **2009**, *79*, 012102.
[34] Y. Zhou, F. Zhang, K. Tvingsted, W. Tian, O. Inganäs, *Appl. Phys. Lett.* **2008**, *93*, 033302.
[35] S. Linic, P. Christopher, D. B. Ingram, *Nat. Mater.* **2011**, *10*, 911.
[36] F. Pschenitzka, Y. Shen, *SID 2012 Digest* **2012**, 1488.
[37] Z. Yu, Q. Zhang, L. Li, Q. Chen, X. Niu, J. Liu, Q. Pei, *Adv. Mater.* **2011**, *23*, 664.
[38] Z. Yu, L. Li, Q. Zhang, W. Hu, Q. Pei, *Adv. Mater.* **2011**, *23*, 4453.
[39] F. C. Krebs, *Org. Electron.* **2009**, *10*, 761.
[40] Organic Electronic Association Roadmap *4th edition*, **2011**, http://www.vdma.org/oe-a (accessed July 2012)
[41] C.-C. Chen, L. Duo, R. Zhu, C.-H. Chung, T.-B. Song, Y. B. Zheng, S. Hawks, G. Li, P. S. Weiss, Y. Yang, *ACS Nano* **2012**, *6*, 7185.
[42] C. Girotto, B. P. Rand, S. Steudel, J. Genoe, P. Heremans, *Org. Electron.* **2009**, *10*, 735.
[43] H. Oh, J. Krantz, I. Litzov, T. Stubhan, L. Pinna, C. J. Brabec, *SOLMAT* **2011**, *95*, 2194.
[44] C. J. Brabec, S. Gowrisanker, J. J. M. Halls, D. Laird, S. Jia, S. P. Williams, *Adv. Mater.* **2010**, *22*, 3839.
[45] T. Ameri, G. Dennler, C. Waldauf, H. Azimi, A. Seemann, K. Forberich, J. Hauch, M. Scharber, K. Hingerl, C. J. Brabec, *Adv. Funct. Mater.* **2010**, *20*, 1592.
[46] H. Hoppe, N. S. Sariciftci, *J. Mater. Res.* **2004**, *19*, 1924.
[47] C. Waldauf, M. C. Scharber, P. Schilinsky, J. Hauch, C. J. Brabec, *J. Appl. Phys.* **2006**, *99*, 104503.
[48] M. T. Lloyd, D. C. Olson, J. J. Berry, N. Kopidakis, M. O. Reese, K. X. Steirer, D. S. Ginley, *35th IEEE PV Specialist Conf.* **2010**, PVSC 2010.
[49] M. O. Reese, A. M. Nardes, B. L. Rupert, R. E. Larsen, D. C. Olson, M. T. Lloyd, S. E. Shaheen, D. S. Ginley, G. Rumbles, N. Kopidakis, *Adv. Funct. Mater.* **2010**, *20*, 3476.
[50] D. Han, H. Kim, S. Lee, M. Seo, S. Yoo, *Opt. Express* **2010**, *18*, A513.
[51] J. Merten, J. M. Asensi, C. Voz, A. V. Shah, R. Platz, J. Andreu, *IEEE Trans. Electron. Dev.* **1998**, *45*, 423.
[52] R. S. Crandall, *J. Appl. Phys.* **1983**, *54*, 7176.